Discovery of Mitogen-Activated Protein Kinase-Interacting Kinase 1 Inhibitors by a Comprehensive Fragment-Oriented Virtual Screening Approach

Julen Oyarzabal,* Natasha Zarich, María Isabel Albarran, Irene Palacios, Manuel Urbano-Cuadrado, Genoveva Mateos, Isabel Reymundo, Obdulia Rabal, Antonio Salgado, Ana Corrionero, Jesús Fominaya, Joaquin Pastor, and James R. Bischoff*

Experimental Therapeutics Programme, Spanish National Cancer Research Centre (CNIO), Melchor Fernandez Almagro 3, 28029 Madrid, Spain

Mitogen-activated protein kinase-interacting kinases 1 and 2 (MNK1 and MNK2) phosphorylate the oncogene eIF4E on serine 209. This phosphorylation has been reported to be required for its oncogenic activity. To investigate if pharmacological inhibition of MNK1 could be useful for the treatment of cancers, we pursued a comprehensive virtual screening approach to rapidly identify pharmacological tools for target validation and to find optimal starting points for a plausible medicinal chemistry project. A collection of 1236 compounds, selected from a library of 42 168 compounds and a database of 18.8 million structures, were assayed. Of the identified hits, 26 were found to have IC_{50} values less than $10 \mu M$ (2.10% hit rate). The most potent compound had an IC_{50} value of 117 nM, and 73.1% of these hits were fragments. The hits were characterized by a high ligand efficiency (0.32−0.52 kcal/mol per heavy atom). Ten different chemical scaffolds were represented, giving a chemotype/hit ratio of 0.38.

Introduction

The initiation of translation factor eIF4E is a partner in a key signaling node that integrates inputs from the PI3K/Akt and Ras/MAPK signal transduction pathways.[1] eIF4E is a component of the eIF4F complex that controls the rate-limiting step of the recruitment of ribosomes to mRNAs. eIF4E binds to the 7-methylguanosine of the mRNA cap which brings the mRNA in proximity to the ribosome in concert with eIF4G, the ribosome binding component of eIF4F.[2] Overexpression of eIF4E is oncogenic and can suppress apoptosis.[3] High levels of eIF4E expression have been linked to the progression of head and neck, colon, breast, and bladder cancer.[1] Wendel et al.[4] demonstrated that the phosphorylaton status of serine 209 is key to eIF4E-driven lymphogenesis. They observed that a catalytically inactive dominant negative form of MNK1,[a] the kinase responsible for the phosphorylation of eIF4E on serine 209, blocks eIF4E-driven lymphomageneis.[4] MNK1 was first identified as a protein kinase that associated and activated by the MAP kinase ERK.[5] Subsequently it was found that MNK1 and MNK2 were the protein kinases responsible for the phosphorylation of eIF4E.[6] Thus far, no other MNK1 or MNK2 substrates have been described. Mice in which both MNK1 and MNK2 have been knocked out in the embryo are viable and show no gross defects,[7] implying that inhibitors targeting MNK1 and MNK2 would be well tolerated. In order to investigate if pharmacological inhibition of MNK1 could be useful for the treatment of cancer, we pursued the following strategy to rapidly identify inhibitors. The goal was to identify pharmacological tools for target validation and at the same time find optimal starting points for medicinal chemistry. Small chemical structures, fragment-like molecules (MW < 300 Da),[8] were preferred because of their potential for rapid expansion and their potential for optimization into leads and then into preclinical candidates. To accelerate the process and minimize costs, our strategy involved the screening of a representative set of chemical structures from our compound collection and a focused set of molecules, fragment-oriented, which were selected using a comprehensive computational approach. Several complementary virtual screening strategies were used, together with in silico physicochemical profiling with a special emphasis on fragment-like structures with optimal predicted solubility (> 100 μM at pH 7.4). In this study we report the identification of 26 novel MNK1 inhibitors, one of which, **29** (Table 1, ETP-45835), can be used as pharmacological tool for MNK1 validation. Compound **29** had IC_{50} for inhibition of MNK1 of 646 nM and was selective against a panel 24 protein kinases. This hit inhibited MNK1 in intact cells, decreasing phosphorylation of eIF4E on serine 209 with an EC_{50} of 4.7 μM. This exercise also identified expandable and viable starting points for medicinal chemistry. In fact, 73.1% of hits were fragments with high ligand efficiency (LE) values,[9] between 0.32 and 0.52 kcal/mol per heavy atom. There were 10 scaffolds represented by the 26 hits which provides an additional qualitative value in terms of diversity, not only from an intellectual property perspective but also considering their physicochemical profiling and related ADME/Tox properties.[10]
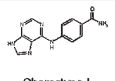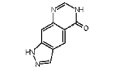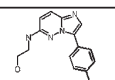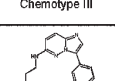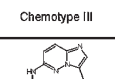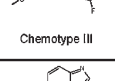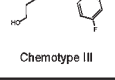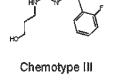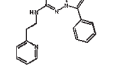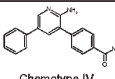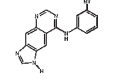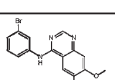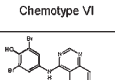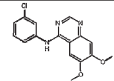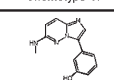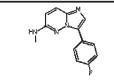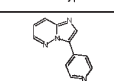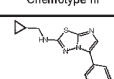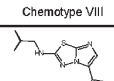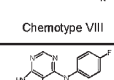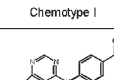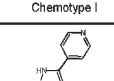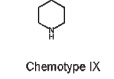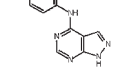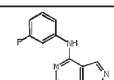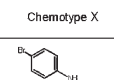
Methods

Fragment-based drug discovery has proven to be a very useful approach in the hit finding process to identify optimal chemistry starting points for drug discovery programs.[11] Fragments with

---

*To whom correspondence should be addressed. For J.O.: phone, +34 91 7328000; fax, +34 91 2246976; e-mail, joyarzabal@cnio.es. For J.R.B.: phone, +34 91 7328000; fax, +34 91 7328051; e-mail, jrbischoff@cnio.es.

[a] Abbreviations: MNK1, mitogen-activated protein kinase-interacting kinase 1; MNK2, mitogen-activated protein kinase-interacting kinase 2; ADME/Tox, adsorption, distribution, metabolism, excretion, and toxicity; VS, virtual screening; PDB, Protein Data Bank; rmsd, root-mean-square deviation; 2D, bidimensional; SSS, substructural searches; ECFP, extended connectivity fingerprints; eMaps, electrostatic maps; LE, ligand efficiency; AML, acute myeloid leukemia; HTS, high-throughput screening; IP, intellectual property; SAR, structure−activity relationship; DB, database; DoE, design of experiments.

Table 1. The 26 Compounds Identified as MNK1 Inhibitors

Structure[a]	ID[c]	IC$_{50}$ (μM)[c]	LE[d]	VS Strategy[e]	Structure[a]	ID[b]	IC$_{50}$ (μM)[c]	LE[d]	VS Strategy[e]
Chemotype I	**8** (ETP-21049)[b]	0.16	0.51	2D Tanimoto	Chemotype VI	**21** (ETP-39900)	0.53	0.41	3D eMaps
Chemotype II	**9** (ETP-21540)[b]	8.17	0.52	2D Tanimoto	Chemotype III	**22** (ETP-41212)[b]	1.53	0.46	FTrees
Chemotype III	**10** (ETP-38766)[b]	2.93	0.40	Rep. CNIO	Chemotype III	**23** (ETP-41214)[b]	4.05	0.43	FTrees
Chemotype III	**11** (ETP-38814)	1.62	0.39	Rep. CNIO	Chemotype III	**24** (ETP-41313)[b]	3.80	0.52	2D Tanimoto
Chemotype III	**12** (ETP-38873)[b]	4.09	0.37	FTrees	Chemotype VIII	**25** (ETP-41567)[b]	1.71	0.43	2D Tanimoto
Chemotype III	**13** (ETP-38890)[b]	2.41	0.38	FTrees	Chemotype VIII	**26** (ETP-41681)[b]	6.18	0.39	FTrees
Chemotype III	**14** (ETP-38919)[b]	3.24	0.37	FTrees	Chemotype I	**27** (ETP-43473)[b]	1.03	0.50	2D Tanimoto
Chemotype III	**15** (ETP-38930)	4.28	0.32	Rep. CNIO	Chemotype I	**28** (ETP-43474)[b]	0.85	0.43	2D Tanimoto
Chemotype IV	**16** (ETP-39189)[b]	5.15	0.34	Rep. CNIO	Chemotype IX	**29** (ETP-45835)[b]	0.65	0.52	2D Tanimoto
Chemotype V	**17** (ETP-39849)	2.80	0.38	FTrees	Chemotype X	**30** (ETP-45852)[b]	0.58	0.52	FTrees
Chemotype VI	**18** (ETP-39855)	0.63	0.40	2D Tanimoto	Chemotype X	**31** (ETP-46146)[b]	1.09	0.50	2D Tanimoto
Chemotype VI	**19** (ETP-39877)	0.12	0.41	3D eMaps	Chemotype X	**32** (ETP-46147)[b]	1.56	0.49	2D Tanimoto
Chemotype VII	**20** (ETP-39888)	1.70	0.41	3D eMaps	Chemotype X	**33** (ETP-46150)[b]	1.35	0.42	2D Tanimoto

[a] All these active compounds were obtained from external sources (more details in Materials and Methods). [b] Identifiers, ETP numbers, for compounds with molecular weight lower than 300 are labeled with letter b as superscript, fragments. [c] IC$_{50}$ values are represented as mean values of two independent experiments. Only differences in pIC$_{50}$ up to 0.6 (SD < 0.5) were considered as reproducible and were maintained (see Materials and Methods for more details). [d] Experimental LE is defined as LE $= \Delta G/N_{HA}$,[9a] where ΔG is the free energy of ligand binding ($\Delta G = -RT \ln K_i$), N_{HA} is the number of heavy atoms in the compound, and K_i values are estimated from the corresponding IC$_{50}$ experimental data and MNK1 assay conditions. ATP concentration was 100 μM, and the K_m for ATP of MNK1 was determined to be 120 μM; thus, $K_i = $ IC$_{50}/(1 + ([ATP]/K_m))$. [e] VS strategy, from the comprehensive approach, driving to its identification as hit.

their low-molecular-mass structure are likely to have high binding energies per unit of molecular mass and in addition are simple structures that allow for enhancement during the multi-factorial lead optimization process.[12] Therefore, we assembled a hit finding collection that is heavily represented by fragments. The compounds represent the medicinal chemistry space defined by our library of molecules together with a complementary set of chemically diverse structures, and a focused set of compounds were selected by a comprehensive fragment-oriented virtual screening. Overall, the selected compounds were skewed 2:1 toward focused fragment-oriented molecules against the representative selection of compounds from the CNIO library.

Virtual Screening (VS). Because of their complementary nature, both structure-based and ligand-based virtual screening strategies were applied to find inhibitors of MNK1. These screens were performed against our CNIO library containing 42 168 unique compounds and our virtual CNIO library composed of 18.8 million unique real compounds, i.e., commercially available or/and reported (e.g., in PubChem, ChemBank, ...). Different but complementary criteria were considered for compound selection and purchase to build our CNIO library of 42 168 compounds: (a) chemistry perspective, druglike compounds, and (b) biological point of view, structures focused on kinases (kinases libraries) and a diverse set of compounds exploring different chemical spaces with a potential biological activity.

The virtual screening was followed by in silico profiling focused on molecular weight and solubility.[13] According to our initial criteria, molecular weight values for selected compounds had to be preferably lower than 300 or fit to a Gaussian curve around this figure, and estimated solubility values, in logarithmic terms, had to be as close as possible to −4 mol/L or higher. This threshold for estimated solubility values was adapted per chemical series once experimental values were available.[14]

Structure-Based Virtual Screening. Crystal structures for both isoforms, MNK1 and MNK2, have been deposited in the Protein Data Bank (PDB). MNK1 and MNK2 have 78% sequence identity within their catalytic domains.[15] This structural information was used to identify compounds fitting the key structural requirements to achieve an optimal binding to MNK1 and MNK2.

Three published crystal structures were considered. Two structures correspond to the apo-form for MNK1 (2hw6.pdb)[15] and MNK2 (2ac3.pdb),[16] both in the inactive conformation (DFG/D out) in which autoinhibition is due to Phe230 (MNK1) or Phe265 (MNK2) from the activation segment, pushing Phe192 (MNK1) or Phe227 (MNK2) away from DFG/D toward the ATP binding site where adenosyl moiety of ATP should be accommodated. The third crystal structure corresponds to the halo form for MNK2 (2hw7.pdb)[15] complexed with staurosporine. Staurosporine binds in the ATP binding site; therefore, kinase active conformation involves a movement toward DFG/D in. There are three key interactions between staurosporine and MNK2: two with residues from hinge region, Glu160 and Met162, and the third between the titrable nitrogen born by staurosporine and Glu209 (Figure 1). In the case of MNK1, only the crystal structure for the inactive form is available in which the size of the ATP binding site is reduced because of Phe192 being pushed toward the ATP binding pocket. Since it is possible that inhibitors may work in either the inactive or active conformations, the initial goal before performing any virtual screening was to elucidate those residues that might be critical for the binding of ligands in both inactive and active conformations.
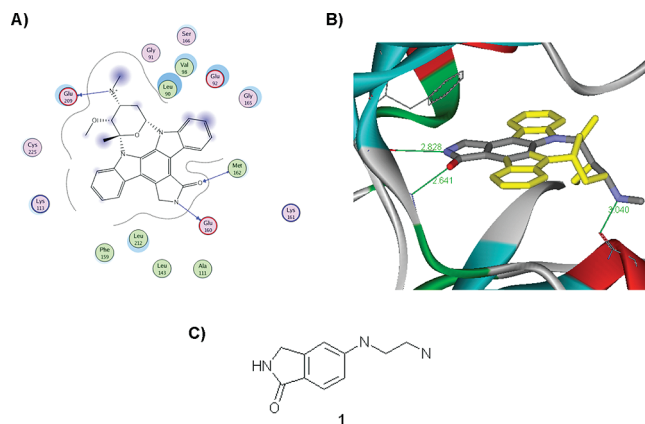

Figure 1. (A) Interaction map, extracted from 2hw7.pdb, where key chemical features from ligand (staurosporine) and MNK2 amino acids involved in binding are highlighted. (B) Minimal substructure, from staurosporine, required to get key interactions with MNK2 (atom type color-coded). (C) Substructure **1** from part B.

The information concerning the ligand−receptor interactions described above for MNK2 and staurosporine was transferred to MNK1 taking into account the degree of sequence identity and structural differences between the inactive and active conformations. The first step was to determine if the docking software GOLD[17] could recapitulate the data published about the MNK2−staurosporine complex (see Materials and Methods for details). Docking was performed without constraints in order to obtain an unbiased result and to explore all possible binding modes of the staurosporine. GOLD was found to reliably redock the crystallographic ligand (rmsd = 0.65 Å); therefore, this was used as the reference for the rest of docking experiments. By use of a similar docking setup, the staurosporine was docked in MNK1, and as expected, it did not fit into the ATP binding pocket of inactive MNK1 probably because of spatial restrictions derived from inactive conformation mentioned above. Consequently, the next step involved the definition of an artificial structure, substructure **1**, with the critical structural requirements for binding identified in the ligand−receptor map of the staurosporine−MNK2 complex described in Figure 1. This substructure **1**, atom type colored in Figure 1, was then docked into MNK1 to check if the previously identified key chemical features, to interact with MNK2, might also bind to MNK1. A consensus result was obtained from docking studies confirming knowledge transfer: three key interactions, two with residues from the hinge region, Leu127 and Gly130, and the third between the titrable nitrogen and backbone from Phe192 (Figure 2) (also quite close to Glu174, equivalent to Glu209 in MNK2, around 5.5 Å). Thus, on the basis of this result, those three key chemical features may be required for ligands to bind to MNK1 and led to the definition of the pharmacophore that can bind to MNK1 (Figure 2). Additional factors were contemplated to fine-tune the pharmacophoric requirements such as exclusion of volume toward the gatekeeper Phe124 in order to avoid a potential clash with this side chain and use of a a larger sphere than usual to define the plausible spatial position for titrable nitrogen. The latter point considered protein plasticity in the transition from the inactive to the active conformation, because if the active conformation takes place, the highlighted interaction predicted with Phe192 backbone might not occur but will occur instead with Glu174.
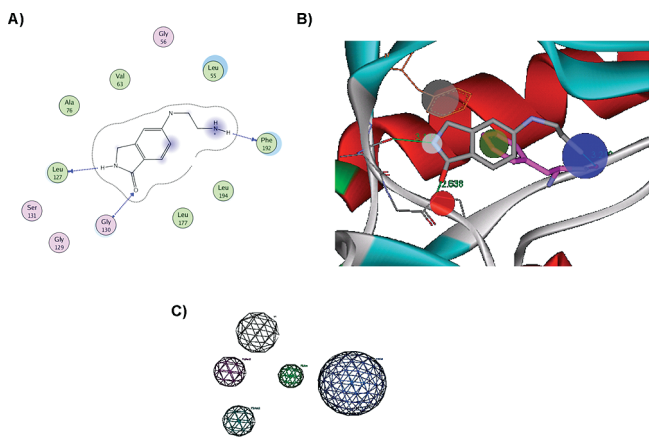
Figure 2. (A) Interaction map, top ranked answer for docked complex, between substructure **1** and MNK1. (B) Key chemical features derived from docked complex, those highlighted in Figure 1B (hydrogen-bond donor in light blue, projection point for hydrogen-bond acceptor in red, and titratable nitrogen in blue) together with aromatic ring (in green) and excluded volume (in gray). (C) 5-points pharmacophore, using CHD scheme, as implemented in MOE (in this case, hydrogen-bond donor is magenta, hydrogen-bond acceptor is light-blue, excluded volume is represented by a gray sphere, aromatic ring is green, and titrable nitrogen is blue).

Once the residues and chemical features that may be critical for binding ligands in active or inactive MNK1 conformations were identified and the pharmacophore was defined (see Materials and Methods for details), pharmacophore fitting was utilized as an alternative to docking in structure-based virtual screening, since implicitly this considers protein plasticity which allows for different alternatives for the titrable nitrogen spatial position and no shape restriction for the ligand; thus, both large and small cavities in the ATP binding site are accepted (active and inactive forms). This pharmacophore was utilized to screen the CNIO library, and a total of 92 compounds were selected that fit all the requirements and possessed an optimal physicochemical in silico profiling.

Ligand-Based Virtual Screening. Four different virtual screening strategies based on ligand-based knowledge were used. Examples of MNK ligands have been published,[18] several of which inhibit MNK as a secondary activity[19] (see Supporting Information Figure SI1). Six known MNK-oriented inhibitors (Figure 3) were selected to use as references for ligand-based virtual screening: the well-known MNK1 inhibitor CGP57380, **2**,[20] together with five additional compounds, MNK1 or/and MNK2 inhibitors **3**,[21] **4**,[22] **5**,[23] **6**,[24] and **7**.[25] The first two ligand-based strategies were utilized to screen both the CNIO library and the proprietary virtual database of external compounds. For the last two cases only the CNIO library was used.

Strategy 1 involved substructural searches together with pharmacophoric requirements (2D SubStruct) (Figure 4). The process involved two sequential steps: (1) identification of compounds bearing the structural requirements defined by the queries; (2) within these compounds, identification of those meeting the previous pharmacophore criteria. In total 249 structures were selected that had all the key pharmacophoric features.

Strategy 2 involved two-dimensional structural similarity (2D Tanimoto). These similarity analyses were based on circular molecular fingerprints using ECFP_6 descriptors,[26] implemented in Pipeline Pilot,[27] that defined the molecular structure using radial atom neighborhoods. These analyses used four compounds as reference structures: two MNK1 inhibitors (structures **2** and **3**) and two MNK2 ligands (compounds **4**

and **5**) (Figure 3). This approach identified 140 molecules as structurally similar to the reference compounds. In the case of the CNIO library, 0.05% of structures with the best Tanimoto similarity values were selected (top values were around 0.40 depending on reference structure) and just 0.0001% of compounds from the virtual CNIO library with best similarity values were selected (top Tanimoto values of around 0.35, again depending on reference compound).

Strategy 3 involved Feature Trees[28] similarity (FTrees, see Materials and Methods for its definition). The six ligands reported in Figure 3 were utilized as references, and those structures with similarity values greater than 0.90, compared to the corresponding reference, were selected. In total, 124 compounds, 0.05% of chemical structures from CNIO library, with the best FTree similarity values were selected.

Strategy 4 involved three-dimensional similarity based on shape[29] and electrostatics[30] (3D eMaps, see Materials and Methods for details). The two reported MNK1 inhibitors were utilized as reference structures (Figure 5). In this case, compounds from CNIO library with the best Tanimoto electrostatic similarity values (top values are around 0.60 and 0.80 for structure **2** and compound **3**, respectively) and a Tanimoto shape similarity value greater than 0.80 were found. A total of 231 compounds were selected.

The above approaches yielded a final set of 836 chemical structures; 73 of these compounds were purchased from commercial suppliers. 70.0% of these selected structures have estimated solubility values greater than 100 μM, and 74.4% of them have a molecular weight lower than 300 (Figure 6).

In addition, a representative set of compounds from the CNIO collection complementing the focused selection was prepared (Rep. CNIO). This selection consisted of 320 compounds representing, from a medicinal chemistry point of view, as many key chemotypes as possible. In order to select this diverse set of compounds, all molecules from our library were computationally fragmented.[10] Then scaffolds were selected on the basis of the following criteria: (i) frequency of representation in the library, (ii) number of fused rings, (iii) number of diversity points, (iv) growing vectors (orientation) for the diversity points, and (v) similarity based on electrostatics[30] and Tanimoto distance (2D Tanimoto), described above, using ATP purine as reference. Then, on the basis of "maximum common substructure" around each selected chemotype, as implemented in Pipeline Pilot,[27] R-group analyses were performed selecting compounds for which the R-groups provide diversity.

Finally, a D-optimal design strategy (see Materials and Methods)[31] was utilized to select an additional set of 80 compounds from the CNIO library. D-Optimal designs can be used in cases in which the data set is composed of discrete molecular structures, thus facilitating the selection a few molecules optimally spanning the domain of interest. This chemometric strategy is particularly useful because it permits the selection of a small number of molecules that cover the entire chemical space represented by our library which can be useful for deriving reliable QSAR (quantitative structure–activity relationship) models. This designed set of informative molecules representing the structural variation in our library collection ensures the reliability of derived models. In addition, once biological data are available for these selected compounds, we can exploit those models using the response surface modeling (RSM)[32] technique to point out trends, favorable directions, and activity regions.[33] All these calculations were performed with SIMCA-P+[34] and MODDE.[35]
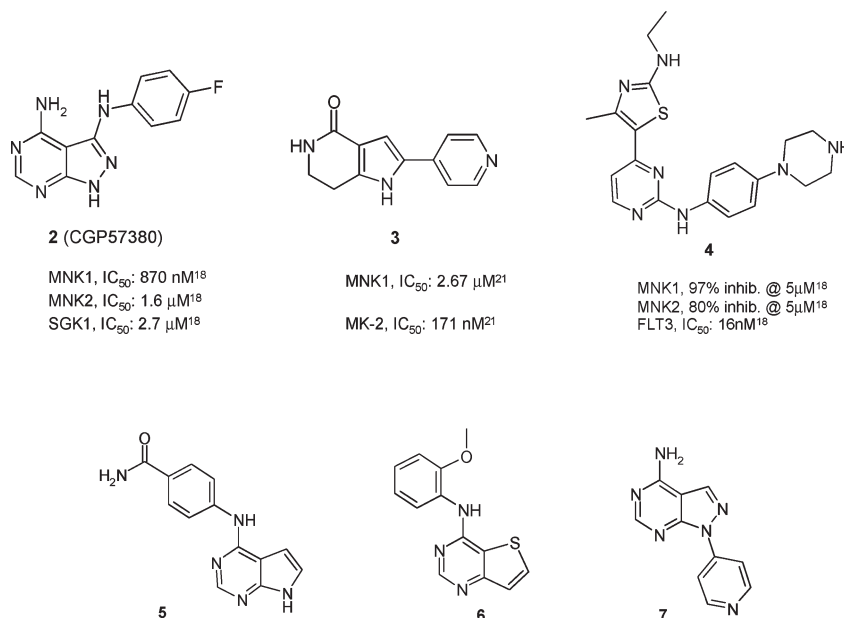
Figure 3. Reported MNK1 and MNK2 inhibitors together with their corresponding activities in those cases where they are explicitly described (only for compounds **2**, **3**, and **4**). Compounds **5**, **6**, and **7** are preferred structures among those reported in their corresponding patents; however, no activity value is described for them.
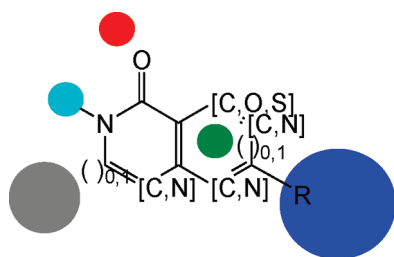

Figure 4. Example of a general query utilized for substructural searches, together with pharmacophoric requirements utilized to refine the final set of selected compounds. Hydrogen-bond donor is in light blue, projection point for hydrogen-bond acceptor in red, and titratable nitrogen in blue together with aromatic ring (in green) and excluded volume (in gray).
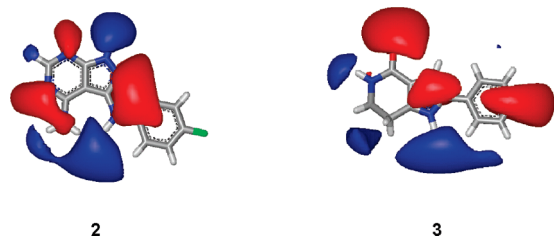

Figure 5. Electrostatic maps, obtained with EON,[30] for the reference structures **2** and **3**.

Results and Discussion

Hit Identification. In total, 1236 compounds selected by methods described above were assayed for the ability to biochemically inhibit MNK1. A total of 26 compounds were confirmed as hits with IC_{50} values less than 10 μM, giving a hit rate of 2.10%. Ten different chemotypes were represented in the 26 hits. In addition, these 26 compounds are characterized by a high ligand efficiency, between 0.32 and 0.52 kcal/mol per heavy atom (Table 1). Six compounds had IC_{50} values superior to that of the reference compound **2**, which had an IC_{50} value of 830 nM in our assay. It is noted that

73.1% of these hits were fragments with a molecular weight less than 300.

In only 1 case out of those 26 hits, compound **28** (ETP-43474), we obtained a selective MNK1 inhibitor vs MNK2; ΔpIC_{50} was greater than 1 log unit. In this case, IC_{50} for MNK1 was 847 nM and bigger than 100 μM for MNK2.

The initial goal of this exercise was to identify a compound that could be used as a pharmacological tool as well as representing a reasonable starting point for medicinal chemistry expansion. Compound **29** met these criteria. This compound was selected by ligand-based virtual screening based on 2D structural similarity within the 18.8 million compounds in the virtual CNIO library of unique real compounds. It was within the top 0.0001% similar structures to reference compound **3** (Figure 3) with a Tanimoto similarity value of 0.30. This compound has an IC_{50} of 646 nM toward MNK1 and a molecular weight of 228, which results in a very high ligand efficiency of 0.52 kcal/mol per heavy atom. Compound **29** was also active toward MNK2, with IC_{50} of 575 nM. In order to determine if **29** was a selective MNK1/2 inhibitor, it was assayed in duplicate against a panel of 24 protein kinases at 5 μM. This panel of 24 kinases included upstream MNK1/2 activating kinases such as B-raf, MEK1, ERK, and p38 to ensure that the observed cellular activity was likely due to MNK inhibition and not to off target activities. Compound **29** was relatively inactive against the 24 kinases tested; in all cases the corresponding percentages of inhibition were less than 16%. These experimental values are in agreement with the estimated "in silico chemogenomics" profiling generated for this compound during its registration process in our database, the Common Chemical Biology Repository (CCBR)[36] (Table 2). Compound **29** had an estimated solubility value greater than 100 μM at pH 7.4.[13] This was confirmed experimentally through a kinetic solubility assay (see Materials and Methods for solubility assay details); its solubility at pH 7.4 was 125 μM.

Five human tumor cell lines were screened to determine if any had activated MNK1. Activation was determined by the level of phosphorylation of the MNK1 on threonines 197 and
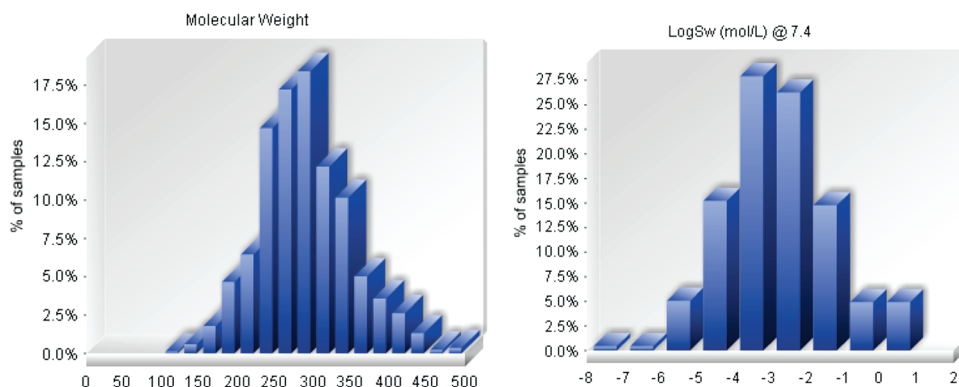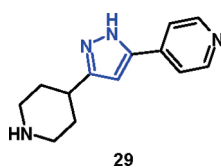
Figure 6. Histograms describing the profiling of a selected set of focused compounds, biased toward molecular weight lower than 300 and optimal estimated solubility values log Sw (mol/L) bigger than −4.0 (100 μM).

Table 2. Profiling Compound **29** against a Panel of 24 Kinases

29

kinase	IC$_{50}$ (nM)[a]	% inhibition at 5 μM[b]	in silico chemogenomics[c]
MNK1	646	87	ND[d]
MNK2	575		ND[d]
AKT1		0	no hit
ARK5		3	ND[d]
B-RAF V600E		9	no hit
CK1-α1		10	ND[d]
DYRK1A		0	ND[d]
EGF-R		1	no hit
ERK1		0	ND[d]
FAK		15	no hit
FGFR1		8	no hit
FLT3		0	no hit
IGF1-R		3	no hit
IKKβ		6	ND[d]
JAK2		0	no hit
KIT		7	no hit
MEK1		5	ND[d]
MET		1	no hit
MST1		0	ND[d]
P38-α		2	ND[d]
PDK1		0	ND[d]
PDGFR-α		1	no hit
PIM1		4	no hit
PIM2		1	ND[d]
RPS6KA1		11	ND[d]
SGK1		7	ND[d]

[a] IC$_{50}$ values are represented as mean values of two independent experiments. Only differences in pIC$_{50}$ up to 0.6 (SD < 0.5) were considered as reproducible and were maintained (see Materials and Methods for more details); [b] Percentages of inhibition as the mean of two independent experiments (see Materials and Methods for additional details). [c] "In silico chemogenomics" profiling is generated for each compound registered in our database, CCBR, where chemical biology data is stored, including in silico.[36] [d] Application scope, from a biological space point of view, for this "in silico chemogenomics" model is defined by 90 kinases. In this case, only 12 overlap with the assayed panel described; thus, estimations could not be determined (ND) for some targets.

202 and on serine 209 of its substrate eIF4E. The five cell lines were from four different tissue origins and included prostate (DU145), breast (T47D), lung (NCI-H460 and A549), and acute myeloid leukemia, AML, (MV4:11). Of the five cell lines screened only DU145 (prostate) and MV4:11 (AML) display high endogenous levels of both phospho-MNK1 and phospho-eIF4E (Figure 7A). Interestingly when the effect of compound **29** was examined on the proliferation of these cell lines, only the MV4:11 cells were affected (Figure 7B). The EC$_{50}$ of the compound was 17 μM. The proliferation of the DU145 cells was not affected (Figure 7B), indicating that activation of MNK1 may not be a determinant of sensitivity in terms of an antiproliferative response to inhibitors of MNK1. Compound **29** was able to decrease the phosphorylation on serine 209 in eIF4E in a dose dependent manner in treated MV4:11 cells (Figure 7C), thus confirming its activity as a pharmacological inhibitor of MNK1. The EC$_{50}$ was estimated to be 4.7 μM. These data suggest that **29** is suitable to use as a tool to study the biological impact of pharmacological inhibition of MNK1 in cellular systems.

On the basis of these results, an assessment of computational approaches utilized for virtual screening was performed from both a quantitative and qualitative point of view (Figure 8). From a quantitative point of view structure-based pharmacophore approaches and D-optimal design strategy (DoE), set of molecules covering the structural diversity in our library collection, did not provide any hits. The reporting of negative results is not customary, but still can be informative. In contrast, using 2D structural similarity retrieved 11 hits, 8 ligands were identified by FTrees, 3 hits were selected by 3D eMaps, and 4 hits came from the representative selection of CNIO library covering diversity from a medicinal chemistry perspective (Figure 8A). Thus, approaches using 2D structural similarity and FTrees yielded good hit rates of 7.86% and 6.45%, respectively (Figure 8B). From a qualitative point of view, considering each virtual screening approach independently, the best results were obtained by using 3D similarity and 2D structural similarity, both with an excellent chemotype/hit ratio of 0.67 and 0.64, respectively (optimal value being 1; more than one hit per strategy is necessary to conclude) (Figure 8C). In this case, the performance obtained by the 2D structural similarity virtual screening approach, from quantitative and qualitative points of view, was superior. This approach had a hit rate of 7.86% and an optimal chemotype/hit ratio of 0.64 (7 different chemotypes out of 11 identified hits). The hits had ligand efficiency values between 0.40 and 0.52 kcal/mol per heavy atom, and 90.9% of those 11 hits were fragments. Compound **29** was identified among 18.8 million structures by this approach.

These results suggest that a compound selection strategy comprising a representative set of compounds from the CNIO collection and a focused set of molecules selected by
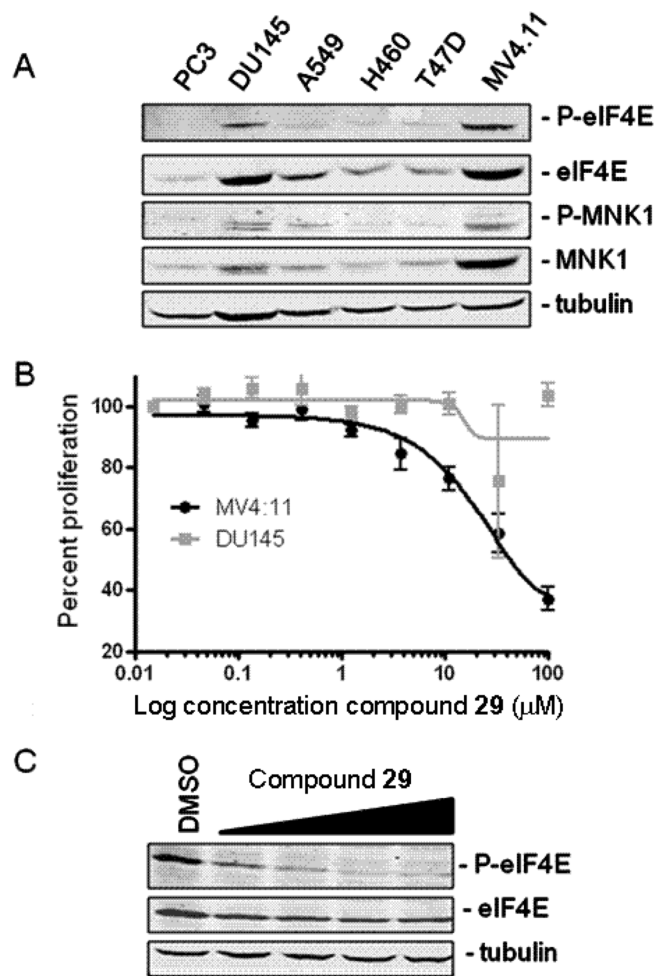
Figure 7. Compound **29** inhibits MNK1 in human tumor cell lines. (A) Determination of the levels of phospho-MNK1 and phospho-eIF4E in human tumor cell lines. Lysates (25 μg of total protein) of the indicated cell lines were analyzed by immunoblotting with anti-P-eIF4E (Ser209), anti-eIF4E, anti-P-MNK1 (Thr197/202), anti-MNK1, and anti-tubulin antibodies as described in Materials and Methods. (B) Effect of treatment with **29** on the proliferation of MV4:11 (solid black circles) and DU145 (solid gray squares). Percent proliferation was calculated from the DMSO treated control. Data from two independent experiments performed in duplicate are presented. (C) MV4.11 cells were treated with DMSO or with 0.21, 0.62, 1.85, or 5.56 μM **29** for 4 h. Phospho-eIF4E, total eIF4E, and tubulin were detected by immunoblotting as described in Materials and Methods. The blot is representative of three independent experiments.

a comprehensive fragment-oriented virtual screening was optimal for the discovery of novel, efficient, and diverse MNK1 inhibitors. More than 70% of the identified MNK1 ligands selected by this strategy were fragments that displayed submicromolar activities and therefore had high ligand efficiency values (LE, 0.32−0.52 kcal/mol per heavy atom). Therefore, considering that typically the primary hits obtained from a fragment screen have biochemical activity of millimolar to high micromolar range with rare exceptions in the 50−200 μM range,[8,37] we can consider these reported results as good. A recent report[11b] by AstraZeneca describes the performance of 12 real cases for which fragment screening was used in its discovery process. These cases included different screening methods, sizes of assayed libraries used, and different target classes and gave hit rates between 0% and 15% (the criteria for hit definition were not reported).

As reported above, the hit rate for identification of MNK1 inhibitors was 2.10%. A hit was defined as a ligand with IC_{50} lower than 10 μM. If a rigorous comparison is performed where only fragments are considered, the hit rate was 2.54%. These hit rates were better than 8 out of those 12 cases reported by AstraZeneca. An additional benchmark used by AstraZeneca was to evaluate the ligand efficacy of fragment hits (frits)[11b] considering the ratio pIC_{50}/N_{HA}. This value was utilized to identify those fragments that should or should not progress in their drug discovery programs. AstraZeneca recommends not pursuing a frit for which the pIC_{50}/N_{HA} ratio is less than 0.25 unless the low value can be clearly understood in terms of its interaction with the target.[11b] In our case the best value for pIC_{50}/N_{HA} (frit) corresponded to 0.37 (details in Table SI1, Supporting Information) which places the results from our fragment-oriented screening campaign in the fourth position relative to the 21 fragment screening campaigns reported by AstraZeneca where frit ratio was explicitly described.[11b] In those cases where pIC_{50}/N_{HA} ratios are less than 0.25 but greater than 0.20, such as the hit bearing the chemotype IV, structural information for the complex target-frit might be critical to clearly understand its interaction with the target in order to reconsider this frit for further optimization. Ligand efficiency values exhibited by our hits, in kcal/mol per heavy atom, were comparable to those recently described as highly efficient hits for which LE values were from 0.30 to 0.50.[38] Advanced fragment hits, such as **29** with a potency profile more similar to those of classical high-throughput screening (HTS) hits, are likely to be easier to progress than traditional fragment hits (usually in the high micromolar) because the key chemical features for its interaction with the critical residues in the binding pocket of MNK1 are already incorporated into the hit molecule.[8]

The identified hits came from 10 different chemical series (Figure 9), which provides an additional value in terms of chemical diversity. From our point of view, the chemotype/hit ratio should also be routinely quantified in screening campaigns, as a third parameter together with hit rate and ligand efficiencies, in order to properly assess results obtained from screening campaigns from a qualitative perspective. In our case the chemotype/hit ratio was 0.38. If only the fragments were considered, then there were 19 hits representing 7 different chemical series, yielding a chemotype/hit ratio for fragments of 0.37.

The chemotypes represented by these hits cover a broad diversity from a structural point of view and include (i) simple five- or six-member heteroaromatic rings, (ii) bicycles with all possible combinations of two fused five- and/or six-member aromatic rings, including heteroaromatics, and (iii) tricycles where different options for five and six-member fused rings are covered. In addition, as Figure 8 shows, all these scaffolds contain more than one diversity point from where they can be functionalized not only to optimize primary activity but also to overcome potential ADME/Tox issues. This diversity in chemotypes provides compounds with similar primary activities but different potential pharmacokinetics and off-target profiles[10] and increases the chance of finding chemotypes with some room from an Intellectual property (IP) perspective. Therefore, obtaining an optimal chemotype/hit ratio is critical to drawing conclusions about the performance of a screening campaign. In theory the higher the ratio is, the better, but a balance with the corresponding hit rate value should be maintained. In a case such as ours, which used
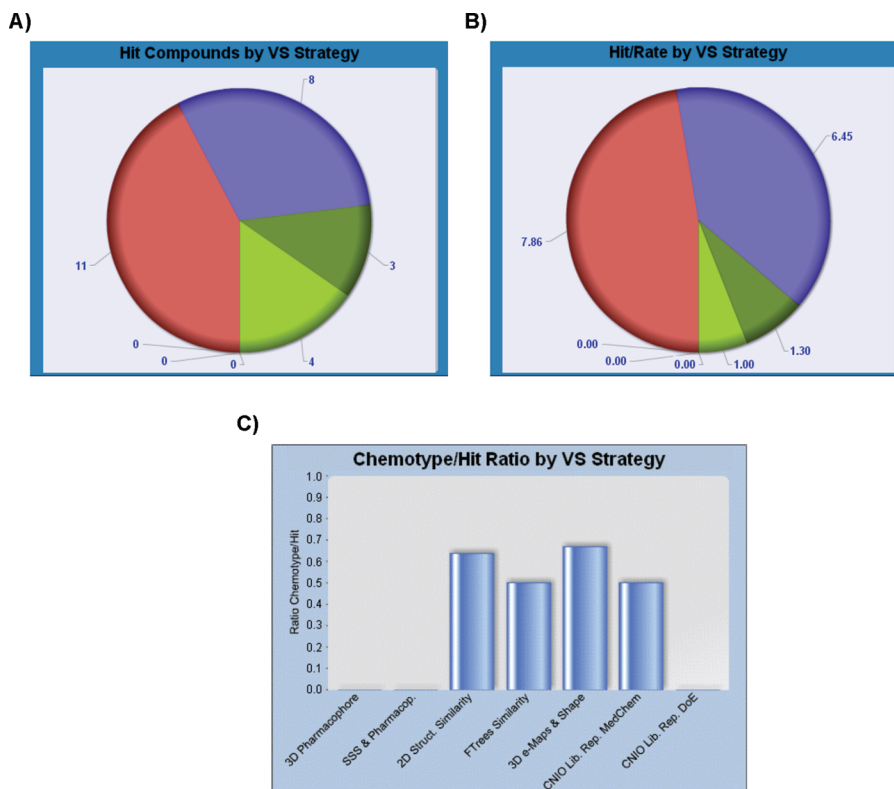
Figure 8. Histograms comparing the performance of computational approaches utilized for this virtual screening. Quantitative point of view: (A) number of hit compounds and (B) hit rate by VS strategy, where each color code represents a different VS strategy: orange, 2D structural similarity; blue, FTrees similarity; dark green, 3D eMaps and shape; green, CNIO library (MedChem representatives). Zero hits were obtained for 3D pharmacophore, SSS and pharmacophore, and CNIO library (DoE representatives). Qualitative assessment was based on (C) chemotype/hit ratio.
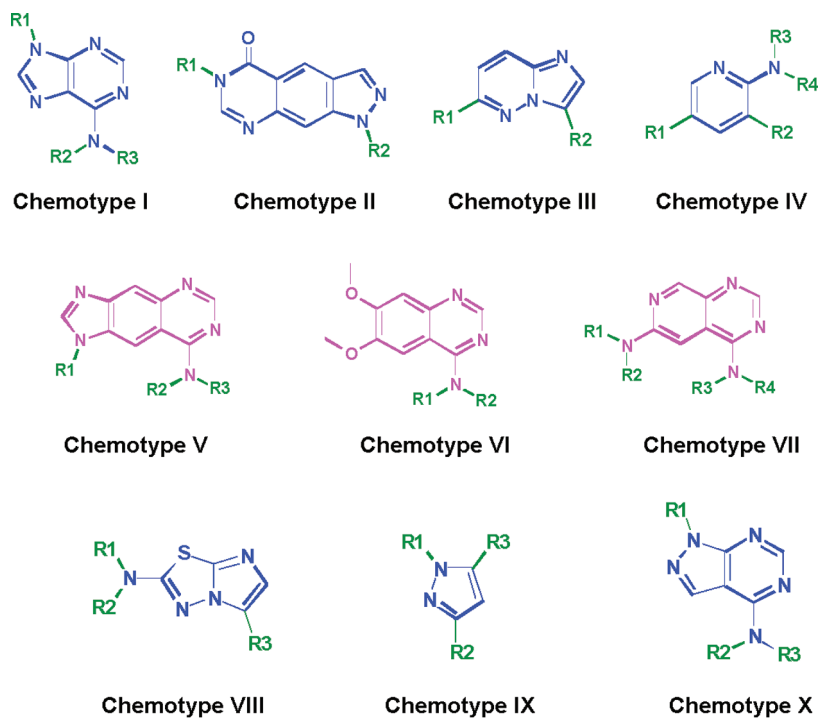
Figure 9. Chemotypes borne by the 26 MNK1 hits reported in Table 1. Those 7 scaffolds in blue are borne by the 19 fragments identified as hits.

commercially available compounds for the screening campaign, the possibility of achieving IP is unlikely. However, because the chemical feasibility is guaranteed and some analogues often are also commercially available, preliminary studies for their structure−activity relationships (SAR) can be easily performed. As a next step, one can use bioisosteric replacements using IP free chemotypes through fragment-hopping strategies[10,12] in order to obtain IP.

Conclusion

The implemented strategy was based on two complementary approaches used to select a limited set of compounds to be used for hit identification: (i) a representative set of compounds from our collection and (ii) a focused set of fragment-oriented molecules, selected from the CNIO library and from a virtual DB of external compounds (18.8 million) by both structure- and ligand-based virtual screening strategies together with an in silico physicochemical and chemogenomics profiling. This comprehensive strategy presented herein for the identification of MNK1 inhibitors gave satisfactory results: 26 inhibitors (hit rate of 2.10%) with very high ligand efficiency (0.32−0.52 kcal/mol per heavy atom) were discovered. More than 73% of these identified hits are fragments. Comparison of these results with recent reports[11b,38] highlights their value. In addition, these 26 inhibitors bear 10 different chemotypes with good diversity, from five- and six-member rings to bicycles and tricycles, and had an acceptable chemotype/hit ratio: 0.38. Six of these hits had a better IC_{50} value than the best reference structure **2**, and the best compound had a binding affinity of 117 nM toward MNK1.

A pharmacological tool compound, **29**, was discovered by the fragment-oriented virtual screening strategy utilized during this hit finding process. Compound **29** is a soluble fragment with very high ligand efficiency (0.52 kcal/mol per heavy atom) and is selective against a panel of 24 kinases including upstream MNK1/2 activating kinases. The compound is active in cells being able to inhibit the phosphorylation of eIF4E with an EC_{50} of 4.7 μM in acute myeloid leukemia cell line (MV4:11) and therefore is suitable to use as a pharmacological tool to evaluate the potential of MNK1/2 inhibition. Thus, our two goals were achieved: the identification of a pharmacological tool for target validation and identification of optimal starting points for a plausible medicinal chemistry program.

These results suggest the applicability of this comprehensive virtual screening approach to rapidly identify not only optimal pharmacological tools for target validation that are potent and selective but also soluble fragments, bearing diverse chemotypes, with high binding affinities that represent optimal starting points for medicinal chemistry.

Materials and Methods

Docking. The Gold 3.1 program[17] was used to carry out docking of staurosporine and substructure **1** to MNK1 (2hw6.pdb)[15] and MNK2 (2hw7.pdb).[15] The binding site was defined using the available experimental information; thus, the docking region used for MNK2 was a 12 Å sphere around the carbon CD2 of Leu212 (atom 2301). GoldScore scoring function was used to rank docking poses without constraints. Per each ligand, the top five best docked structures out of 20 independent genetic algorithm runs were retrieved. For validation purposes, we compared the data for staurosporine docked to MNK2 with the corresponding crystal structure (PDB entry 2hw7.pdb).[15] The rmsd between reported staurosporine and the pose obtained, unique consensus answer, is 0.65 Å. Once the setting of GOLD, using previous complex, was validated, then a similar setup was utilized with MNK1 as receptor. In this case, the binding site was defined using a 12 Å sphere around the carbon CD1 of Leu177 (atom 2234). Again, GoldScore scoring function was used to rank docking poses without constraints. Per each ligand, the top five best docked structures out of 20 independent genetic algorithm runs were retrieved; in this case, the consensus answer in the top three ranked results out of the five.

Pharmacophore. On the basis of the proposed binding mode for substructure **1**, the key chemical features providing critical interactions with MNK1 were identified as well as exclude volumes; therefore, the corresponding pharmacophore annotation was performed. In this case, by using MOE,[39] the charged-hydrophobic-direction (CHD) scheme was utilized to build a 5-points pharmacophore.

Sampling the Conformational Space. Software developed by OpenEye,[40] Omega,[41] was utilized to explore the conformational space around each molecule within an energetic window of 25 kcal/mol, where conformers with a root of mean square deviation (rmsd) of > 0.4 Å are stored, until a maximum of 500, to ensure adequate and diverse conformational representation. Thus, multiconformer databases for CNIO library and selected compounds from substructural searches were ready for pharmacophore query searching.

Feature Trees Similarity. Features Trees (FTrees)[28] are descriptors that represent the molecule as a reduced graph. The graph encodes functional groups and rings to single nodes. FTree descriptor is a rather fuzzy description of the molecule, ignoring its three-dimensional structure and chirality. It preserves only the overall topology of the FTree nodes, but within the nodes FTrees compare only property profiles without taking into account the exact positions of certain functionalities. FTrees focus basically only on the presence or absence of certain functionalities in roughly the right position, and thus, it is able to detect remote similarities.

3D Similarity Analysis. Once all conformers per each structure were generated, we had to align them with the corresponding reference compound before doing any further analysis. In this case, we utilize the ROCS (rapid overlay of chemical structures) package,[29] by Open Eye, to perform the alignment because this is a fast and accurate method for superimposing molecules. Shape similarity can be determined, in part, by comparing the shapes of those molecules. This effectively reduces to calculating the overlap volume between two molecules and has been previously reported. Once the overlap has been optimized, the shape similarity may be computed by Tanimoto equation. However, ROCS does not contain an accurate notion of charge distribution and therefore is not a complete solution to the search for molecular similarity. The electrostatic fields of molecules can be calculated and the similarity between fields expressed as the electrostatic Tanimoto. Electrostatics Tanimoto (ET) scores are calculated using the EON program,[30] by Open Eye. Molecules are superimposed using ROCS, providing shape similarities vs reference compound, and electrostatic potentials are calculated using OpenEye's ZAP Poisson−Boltzmann solver implemented in EON. In this case ET is calculated using an external dielectric of 80, thus accounting for dampening of electrostatic field by aqueous solvent, and may better represent the field experienced upon binding a protein.[42] A normalized shape Tanimoto of unity indicates that the molecules are identical, and the Tanimoto tends to zero as molecules become less similar; the electrostatic Tanimoto ranges from −0.3 to +1, indicating dissimilar and similar electrostatic fields.[40] From the CNIO library, 0.30% top ranking compounds, in terms of shape and electrostatics, are selected.

Design of Experiments (DoE). Three principal components (scores $t[1]$, $t[2]$, and $t[3]$) derived from 315 1D and 2D descriptors (including electrotopological state keys, VSA descriptors, and molecular property counts as implemented in Pipeline Pilot)[27] cover 73.1% of the chemical space defined by CNIO library (42 168 compounds). Onion design is an addition to the design of experiments toolbox, and MODDE software[35] is utilized. An onion design represents the experimental space as comprising a number of subspaces. The experimental domain is constructed from score variables derived from a multivariate projection, principal component analysis (PCA), model. Here we refer to such a subspace as a "layer" or "shell". A local design is associated with a layer. These local designs can be classical or D-optimal. We utilize onion design in statistical molecular design; thus, a subset of molecules is selected to represent the variation across the entire candidate set, the whole CNIO library. One critical step in the generation of an onion design

is the division of the design space into smaller parts. The subdivision emanates from the defined center-point, and in our case, by use of scores variables drawn from the PCA projection model, the subset selection is distance-based. This means that each subdivision of the experimental domain can be interpreted as a spherical "shell" surrounding the center-point coordinate. Thus, the structure of these designs resembles an onion. The onion D-optimal design was based on those three scores obtained from the PCA described above, covering 73.1% of the total variance, and three layers were utilized. As regression, in this RSM application, a linear model was selected to be supported in each layer, with the exception of the outermost one, which supports a quadratic model. After generating a number of tentative D-optimal designs, tailored to the various layers, MODDE displays the recommended number of runs per each layer. This proposed set of selected compounds, runs, is designed by G-efficiency. Thus, in our case, the final onion D-optimal design had 80 compounds.

Biochemical Assays. MNK1 and MNK2 were purchased from CARNA Biosciences. The biochemical assay activity used the ADP Hunter assay kit (DiscoveRx Corp., catalogue no. 90-0077 which determines the amount of ADP as direct product of the kinase catalytic activity. The reaction mixture consisted of 15 mM HEPES, pH 7.4, 20 mM NaCl, 1 mM EGTA, 0.02% Tween 20, 10 mM $MgCl_2$, and 0.1 mg/mL bovine γ-globulins. MNK1 or MNK2 were included at a final concentration of 4 μg/mL (MNK1) or 0.7 μg/mL (MNK2). The final concentration of ATP (Sigma) was 100 μM. The peptide substrate (TATKSGSTTKNR) was designed from the amino acid residues surrounding serine 209 of human eIF4E and was included at a final concentration of 300 μM. The final reaction mixture was incubated for 60 min at 30 °C. The assays were performed in 384-well plates (Corning 3575 or 3573). The product of the coupled reactions was the release of the fluorescent product resorufin and was measured with a multilabel HTS counter ENVISION (PerkinElmer) using an excitation filter at 550 nm and an emission filter at 590 nm. The protein kinase assays, with the exceptions of MNK1 and MNK2, depicted in Table II of Supporting Information were performed at ProQinase, GmbH; visit www.proquinase.com for details.

Cell Lines, Immunoblots, and Proliferation Assays. Cell lines were obtained from the American Type Culture Collection (ATTC; Manassas, VA). MV4:11 (human AML), T47D (human breast cancer), NCI-H460, A549 (human lung cancer), DU145 (human prostate cancer) cell lines were maintained in RPMI 1640 (Sigma). All media were supplemented with 10% fetal bovine serum (Sigma) and antibiotics–antimycotics (Gibco). Cells were maintained in a humidified incubator at 37 °C with 5% CO_2 and passaged when confluent using trypsin/EDTA. For immunoblotting experiments, cells were plated in six-well tissue culture plates at 3×10^5 cells/well in 2 mL of medium. Rabbit polyclonal antibodies to phospho-eIF4E (S-209) (no. 9741), eIF4E (no. 9742), phospho-MNK1 (Thr197/202) (no. 2111), and MNK1 (no. 2195) proteins were purchased from Cell Signaling Technology (Beverly, MA). Antitubulin monoclonal antibody was purchased from Sigma-Aldrich. MNK1 inhibitors were dissolved in DMSO at 10 mmol/L, and aliquots were stored at −80 °C. Stock solutions were diluted to the desired final concentrations with growth medium just before use. Following treatment cells were washed with ice-cold phosphate-buffered saline (PBS) and lysed in buffer containing 50 mM Tris, pH 7.5, 150 mM NaCl, 1% NP-40 supplemented with protease and phosphatase inhibitors (Roche). Cell lysates were clarified by centrifugation at 12000g for 15 min at 4 °C, resolved by SDS–polyacrylamyde gel electrophoresis (PAGE), and subsequently transferred onto nitrocellulose membranes. Blots were probed with the indicated primary and appropriate Alexa Fluor 680 conjugated or Alexa Fluor 800 conjugated secondary antibodies (Molecular Probes) and were visualized and quantified using the Odyssey infrared imaging system (Li-Cor, Biosciences). For proliferation assays cells were harvested just prior to reaching confluency, counted with a hemocytometer, and diluted with media. Cells were then seeded in 96-well microtiter plates at a density between 1000 and 4000 cells/well, depending on the cell size. Cells were incubated for 24 h before adding the compounds. Compounds were weighed out and diluted with DMSO to a final concentration of 10 mM. From here a "mother plate" with serial dilutions was prepared at 200× the final concentration in the culture. The final concentration of DMSO in the tissue culture media should not exceed 0.5%. The appropriate volume of the compound solution (usually 2 μL) was added automatically (Beckman FX 96 tip) to media to make it up to the final concentration for each drug. The medium was removed from the cells and replaced with 0.2 mL of medium containing the compound. Each concentration was assayed in duplicate. Two sets of control wells were left on each plate, containing either medium without drug or medium with the same concentration of DMSO. A third control set was obtained with the cells untreated just before adding the drugs (seeding control, number of cells starting the culture). Cells were exposed to the compounds for 72 h and then processed for MTT colorimetric readout.

Solubility Assay. In 1 mL vials, test compound (5 μL of a 10 mM stock solution in DMSO) was diluted with 245 μL of pH 7.4 PBS buffer (A), pH 4 10 mM phosphate buffer (B), or 10 mM HCl (C). Each mixture was prepared in duplicate. After being stirred at 30 rpm for 24 h at room temperature, mixtures were filtered through 0.45 μm polypropylene filters and analyzed by LC−MS (method 1, details in Supporting Information). Solubility was estimated by comparing area integrals of chromatograms (254 nm) with those of a standard sample prepared by diluting 5 μL of test compound solution (10 mM in DMSO) with 245 μL of methanol−dimethyl ether 50:50 (v:v) and analyzed by the same LC−MS method. The integral area of the standard samples was given a 200 μM solubility value.

Compounds. Tested compounds were purchased from seven different vendors: ChemDiv, BioFocus, Calbiochem, Life Chemicals, Asinex, Enamine, and Aurora. The vendors had verified that each compound had ≥95% purity by liquid chromatography−mass spectrometry (LC−MS) or/and nuclear magnetic resonance (NMR) experiments. An internal quality control was performed for those active molecules, 26 hit compounds; thus, evidence of their purity was checked by LC−MS confirming that in all cases compounds are ≥91% pure (details in Supporting Information, Table SI2).

Supporting Information Available: Quality control for hits, HPLC−MS methods, and additional details for hit compounds. This material is available free of charge via the Internet at http://pubs.acs.org.

References

(1) De Benedetti, A.; Graff, J. R. eIF-4E expression and its role in malignancies and metastases. *Oncogene* **2004**, *23*, 3189–3199.

(2) Gingras, A. C.; Raught, B.; Sonenberg, N. eIF4 initiation factors: effectors of mRNA recruitment to ribosomes and regulators of translation. *Annu. Rev. Biochem.* **1999**, *68*, 913–963.

(3) Polunovsky, V. A.; Rosenwald, I. B.; Tan, A. T.; White, J.; Chiang, L.; Sonenberg, N.; Bitterman, P. B. Translational control of programmed cell death: eukaryotic translation initiation factor 4E blocks apoptosis in growth-factor-restricted fibroblasts with physiologically expressed or deregulated Myc. *Mol. Cell. Biol.* **1996**, *16*, 6573–6581.

(4) Wendel, H.-G.; Silva, R. L. A.; Malina, A.; Mills, J. R.; Zhu, H.; Ueda, T.; Watanabe-Fukunaga, R.; Fukunaga, R.; Teruya-Feldstein, J.; Pelletier, J.; Lowe, S. W. Dissecting eIF4E action in tumorigenesis. *Genes Dev.* **2007**, *21*, 3232–3237.

(5) (a) Waskiewicz, A. J.; Flynn, A.; Proud, C. G.; Cooper, J. A. Mitogen-activated protein kinases activate the serine/threonine

kinases Mnk1 and Mnk2. *EMBO J.* **1997**, *16*, 1909–1920. (b) Fukunaga, R.; Hunter, T. MNK1, a new MAP kinase-activated protein kinase, isolated by a novel expression screening method for identifying protein kinase substrates. *EMBO J.* **1997**, *16*, 1921–1933.

(6) Waskiewicz, A. J.; Johnson, J. C.; Penn, B.; Mahalingam, M.; Kimball, S. R.; Cooper, J. A. Phosphorylation of the cap-binding protein eukaryotic translation initiation factor 4E by protein kinase Mnk1 in-vivo. *Mol. Cell. Biol.* **1999**, *19*, 1871–1880.

(7) Ueda, T.; Watanabe-Fukunaga, R.; Fukuyama, H.; Nagata, S.; Fukunaga, R. Mnk2 and Mnk1 are essential for constitutive and inducible phosphorylation of eukaryotic initiation factor 4E but not for cell growth or development. *Mol. Cell. Biol.* **2004**, *24*, 6539–6549.

(8) Makara, G. M. On sampling of fragment space. *J. Med. Chem.* **2007**, *50*, 3214–3221.

(9) (a) Hopkins, A. L.; Groom, C. R.; Alex, A. Ligand efficiency: a useful metric for lead selection. *Drug Discovery Today* **2004**, *9*, 430–431. (b) Abad-Zapatero, C.; Metz, J. T. Ligand efficiency indices as guideposts for drug discovery. *Drug Discovery Today* **2005**, *10*, 464–469.

(10) Oyarzabal, J; Howe, T.; Alcazar, J.; Andres, J. I.; Alvarez, R. M.; Dautzenberg, F.; Iturrino, L.; Martinez, S.; Van der Linden, I. Novel approach for chemotype hopping based on annotated databases of chemically feasible fragments and a prospective case study: new melanin concentrating hormone antagonists. *J. Med. Chem.* **2009**, *52*, 2076–2089.

(11) (a) Alex, A. A.; Flocco, M. M. Fragment-based drug discovery: What has it achieved so far? *Curr. Top. Med. Chem.* **2007**, *7*, 1544–1567. (b) Albert, J. S.; Blomberg, N.; Breeze, A. L.; Brown, A. J. H.; Burrows, J. N.; Edwards, P. D.; Folmer, R. H. A.; Geschwindner, S.; Griffen, E. J.; Kenny, P. W.; Nowak, T.; Olson, L.-L.; Sanganee, H.; Shapiro, A. An integrated approach to fragment-based lead generation: philosophy, strategy and case studies from AstraZeneca's drug discovery programmes. *Curr. Top. Med. Chem.* **2007**, *7*, 1600–1629.

(12) Ji, H.; Stanton, B. Z.; Igarashi, J.; Li, H.; Martasek, P.; Roman, L. J.; Poulos, T. L.; Silverman, R. B. Minimal pharmacophoric elements and fragment hopping, an approach directed at molecular diversity and isozyme selectivity. Design of selective neuronal nitric oxide synthase inhibitors. *J. Am. Chem. Soc.* **2008**, *130*, 3900–3914.

(13) *ACD/Solubility DB*, version 12.0; Advanced Chemistry Development, Inc.: Toronto, Canada, 2008; http://www.acdlabs.com.

(14) Oyarzabal, J; Pastor, J.; Howe, T. Optimizing the performance of in silico ADMET general models according to local requirements: MARS approach. Solubility estimations as case study. *J. Chem. Inf. Model.* **2009**, *49*, 2837–2850.

(15) Jauch, R.; Cho, M. K.; Jäkel, S.; Netter, C.; Schreiter, K.; Aicher, B.; Zweckstetter, M.; Jäckle, H.; Wahl, M. C. Mitogen-activated protein kinases interacting kinases are autoinhibited by a reprogrammed activation segment. *EMBO J.* **2006**, *25*, 4020–4032.

(16) Jauch, R.; Wahl, M. C.; Netter, C.; Jäkel, S.; Schreiter, K.; Aicher, B.; Jäckle, H. Structures of MNK2 Kinase Domain and MNK2 (D228G) Kinase Domain. Unpublished data deposited in the Protein Data Bank (PDB).

(17) Jones, G.; Willett, P.; Glen, R. C.; Leach, A. R.; Taylor, R. Development and validation of a genetic algorithm for flexible docking. *J. Mol. Biol.* **1997**, *267*, 727–748.

(18) Kinase Knowledgebase (KKB) is available from Eidogen-Sertanty, Inc. at http://www.eidogen-sertanty.com (accessed May 2009).

(19) Karaman, M. W.; Herrgard, S.; Treiber, D. K.; Gallant, P.; Atteridge, C. E.; Campbell, B. T.; Chan, K. W.; Ciceri, P.; Davis, M. I.; Edeen, P. T.; Faraoni, R.; Floyd, M.; Hunt, J. P.; Lockhart, D. J.; Milanov, Z. V.; Morrison, M. J.; Pallares, G.; Patel, H. K.; Pritchard, S.; Wodicka, L. M.; Zarrinkar, P. P. A quantitative analysis of kinase inhibitor selectivity. *Nat. Biotechnol.* **2008**, *26*, 127–132.

(20) Knauf, U.; Tschopp, C.; Gram, H. Negative regulation of protein translation by mitogen-activated protein kinase-interacting kinases 1 and 2. *Mol. Cell. Biol.* **2001**, *21*, 5500–5511.

(21) Anderson, D. R.; Meyers, M. J.; Vernier, W. F.; Mahoney, M. W.; Kurumbail, R. G.; Caspers, N.; Poda, G. I.; Schindler, J. F.; Reitz, D. B.; Mourey, R. J. Pyrrolopyridine inhibitors of mitogen-activated protein kinase-activated protein kinase 2 (MK-2). *J. Med. Chem.* **2007**, *50*, 2647–2654.

(22) Wang, S.; Wood, G.; Duncan, K.; Meades, C.; Gibson, D.; Mclachlan, J.; Fischer, P. Preparation of 2-Substituted 4-Thiazolyl-pyrimidines as Protein Kinase Inhibitors with Improved Solubility Properties. Patent WO05116025 A2, 2005; 216 pp.

(23) Jaekel, S.; Reuter, T.; Murfin, S.; Coulter, T. S.; Taylor, S. Pyrrolopyrimidines for Pharmaceutical Compositions. Patent WO08006547 A2, 2008; 60 pp.

(24) Aicher, B.; Coulter, T. S.; Jaekel, S.; Kelter, A.-R.; Murfin, S.; Reuter, T.; Taylor, S. Thienopyrimidines Having MNK1/MNK2 Inhibiting Activity for Pharmaceutical Compositions. Patent WO07115822 A1, 2007; 95 pp.

(25) Coulter, T. S.; Taylor, S.; Murfin, S.; Thammalaksa, V.; Aicher, B.; Jaekel, S.; Reuter, T. Preparation of Pyrazolopyrimidines as Inhibitors of Kinase Activity. Patent WO06066937 A2, 2006; 122 pp.

(26) (a) Bender, A.; Glen, R. C. A discussion of measures of enrichment in virtual screening: comparing the information content of descriptors with increasing levels of sophistication. *J. Chem. Inf. Model.* **2005**, *45*, 1369–1375. (b) Bender, A.; Mussa, H. Y.; Reiling, S.; Glen, R. C. Similarity searching of chemical databases using atom environment descriptors (MOLPRINT 2D): evaluation of performance. *J. Chem. Inf. Model.* **2004**, *44*, 1708–1718. (c) Glen, R. C.; Bender, A.; Arnby, C. H.; Carlsson, L.; Boyer, S.; Smith, J. Circular fingerprints: flexible molecular descriptors with applications from physical chemistry to ADME. *IDrugs* **2006**, *49*, 199–204.

(27) *Pipeline Pilot*, version 7.5; Accelrys, Inc. (10188 Telesis Court, Suite 100, San Diego, CA 92121); http://accelrys.com/.

(28) *FTrees*, version 2.0. BioSolveIT GmbH (An der Ziegelei 79, 53757 Sankt Augustin, Germany); http://www.biosolveit.de.

(29) Grant, J. A.; Gallardo, M. A.; Pickup, B. T. A fast method of molecular shape comparison. A simple application of Gaussian description of molecular shape. *J. Comput. Chem.* **1996**, *17*, 1653–1666.

(30) (a) Nicholls, A.; MacCuish, N. E.; MacCuish, J. D. Variable selection and model validation of 2-D and 3-D molecular descriptors. *J. Comput.-Aided Mol. Des.* **2004**, *18*, 451–474. (b) Nicholls, A.; Grant, A. J. Molecular shape and electrostatics in the encoding of relevant chemical information. *J. Comput.-Aided Mol. Des.* **2005**, *19* (9−10), 661–686.

(31) (a) Mitchell, T. J. An algorithm for the construction of "D-optimal" experimental designs. *Technometrics* **1974**, *16*, 203–210. (b) St. John, R. C.; Draper, N. R. D-Optimality for regression designs: a review. *Technometrics* **1975**, *17*, 15–23. (c) Dumouchel, W.; Jones, B. A simple bayesian modification of D-optimal designs to reduce dependence on an assumed model. *Technometrics* **1994**, *36*, 37–47.

(32) Myers, R. H. *Response Surface Methodology*; Allyn and Bacon Inc.: Boston, MA, 1971.

(33) Giraud, E.; Luttmann, C.; Lavelle, F.; Riou, J.-L.; Mailliet, P.; Laoui, A. Multivariate data analysis using D-optimal designs, partial least squares, and response surface modeling: a directional approach for the analysis of farnesyltransferase inhibitors. *J. Med. Chem.* **2000**, *43*, 1807–1816.

(34) *SIMCA-P+*, version 11.0; Umetrics AB (Box 7960, SE-907 19 Umea, Sweden); www.umetrics.com.

(35) *MODDE*, version 8.0; Umetrics AB (Box 7960, SE-907 19 Umea, Sweden); www.umetrics.com.

(36) Urbano-Cuadrado, M.; Rabal, O.; Oyarzabal, J. Centralizing discovery information: from logistics to knowledge at a public organisation. *Comb. Chem. High Throughput Screening*, in press.

(37) Hajduk, P.; Huth, J. R.; Fesik, S. W. Druggability indices for protein targets derived from NMR-based screening data. *J. Med. Chem.* **2005**, *48*, 2518–2525.

(38) Katritch, V.; Jaakola, V. P.; Lane, J. R.; Lin, J.; Ijzerman, A. P.; Yeager, M.; Kufareva, I.; Stevens, R. C.; Abagyan, R. Structure-based discovery of novel chemotypes for adenosine A(2A) receptor antagonists. *J. Med. Chem.* **2010**, *53*, 1799–1809.

(39) *Molecular Operating Environment (MOE)*; Chemical Computing Group Inc. (1010 Sherbrooke St. W, Suite 910, Montreal, Quebec, Canada); http://www.chemcomp.com.

(40) OpenEye Scientific Software Inc. (9 Bisbee Court, Suite D, Santa Fe, NM 87508); http://www.eyesopen.com.

(41) Boström, J. Reproducing the conformations of protein-bound ligands: a critical evaluation of several popular conformational searching tools. *J. Comput.-Aided. Mol. Des.* **2001**, *15*, 1137–1152.

(42) Jennings, A.; Tennant, M. Selection of molecules based on shape and electrostatic similarity: proof of concept of "electroforms". *J. Chem. Inf. Model.* **2007**, *47*, 1829–1838.